Coarse-Grained and Reverse-Mapped United-Atom Simulations of Long-Chain Atactic Polystyrene Melts: Structure, Thermodynamic Properties, Chain Conformation, and Entanglements

Theodora Spyriouni,[†] Christos Tzoumanekas,[‡,§] Doros Theodorou,*[,†,‡,§] Florian Müller-Plathe,[⊥] and Giuseppe Milano[||]

Department of Materials Science and Engineering, School of Chemical Engineering, National Technical University of Athens, 9 Heroon Polytechniou Street, Zografou Campus, Athens GR 15780, Greece, Institute of Physical Chemistry, NRCPS "Demokritos", Aghia Paraskevi Attikis, 153 10 Athens, Greece, and Dutch Polymer Institute (DPI), P.O. Box 902, 5600 AX Eindhoven, The Netherlands, Eduard-Zintl-Institut für Anorganische und Physikalische Chemie, Technische Universität Darmstadt, Petersenstrasse 20, D-64287 Darmstadt, Germany, Dipartimento di Chimica, Università di Salerno, I-84084 via Ponte don Melillo Fisciano (SA), Italy

Received January 12, 2007; Revised Manuscript Received March 12, 2007

ABSTRACT: A coarse-grained model of atactic polystyrene, in which *meso* and *racemo* diads are represented as single "superatoms," parametrized using Iterative Boltzmann Inversion, has been subjected to connectivity-altering Monte Carlo simulations in order to simulate monodisperse atactic polystyrene melts of molar mass up to 210000 g mol^{-1} at 500 or 413 K and 1 bar. Analysis of the Monte Carlo results reveals excellent equilibration of chain conformations at all length scales. Chain dimensions, as determined from the mean square end-to-end distance, the mean square radius of gyration, and simulated Kratky plots of the single-chain scattering function, are in excellent agreement with experiment. The equilibrated long-chain configurations are reduced to entanglement networks via topological analysis with the CReTA algorithm. The resulting Kuhn length of primitive paths provides an excellent estimate of the molar mass between entanglements and of the entanglement tube diameter extracted from plateau modulus measurements. The distribution of strand lengths between entanglements, when appropriately reduced, follows the same master curve as previously determined distributions of polyethylene, *cis*-1,4 polybutadiene, and poly(ethylene terephthalate). A new strategy is introduced for reverse mapping the long-chain coarse-grained configurations into detailed united-atom configurations in a manner that preserves the sequence of diad types along the chains. This strategy employs local "flip" Monte Carlo moves to relax the reverse-mapped configurations. Relaxation starts using bonded interactions only, and proceeds by gradually introducing nonbonded interactions. Final relaxation is achieved via short-time canonical molecular dynamics simulation. Predicted wide-angle X-ray diffraction patterns from reverse-mapped configurations are indistinguishable from those of short-chain melts equilibrated directly in the united atom representation using molecular dynamics, and in favorable agreement with experiment. Distributions of torsion angles and pairs of successive torsion angles in the reverse-mapped configurations exhibit some deviations from the corresponding distributions of directly equilibrated short-chain united atom melts and from experimental NMR measurements.

1. Introduction

Vinyl polymers such as polypropylene, poly(vinyl chloride), and polystyrene (PS) are the most common commercial plastics. Developing efficient and reliable molecular simulation techniques for these polymers is highly desirable, as it would help in understanding, predicting, and ultimately controlling the relations between structure, properties, processing, and performance of bulk phases, as well as of films, blends, (nano) composites, and other products based on them.

A serious challenge for polymer simulators is presented by the long length and time scales characterizing structure and dynamics in actual applications. In the melt state, Monte Carlo (MC) simulation offers the possibility of designing moves that permit a more vigorous sampling of configuration space than molecular dynamics (MD). A class of connectivity-altering MC algorithms,[1,2] involving elementary moves that operate on single chains or pairs of chains, has been very useful in equilibrating long-chain polymer melts at all length scales. The equilibration time for these algorithms scales much more favorably with chain length than for MD, allowing savings of many orders of magnitude for systems with molecular weight distributions comparable to those encountered in commercial polymer products and in most experimental studies. However, direct application of connectivity-altering moves to systems possessing bulky, inflexible moieties along their backbones (poly(ethylene terephthalate)) or as side chains (PS) leads to very low acceptance rates when implemented in conjunction with a detailed atomistic model. This difficulty can be overcome by resorting to coarse-grained (CG) models, which involve much fewer degrees of freedom for the representation of the material and therefore employ softer, smoother effective nonbonded interactions. Thus, a promising strategy that has emerged for such polymers is to (a) reduce the atomistic system into a coarse-grained one, (b) equilibrate at the coarse-grained level with the connectivity-altering MC algorithms, and (c) reverse-map the equilibrated coarse-grained configurations into appropriate ato-

* Corresponding author. E-mail: doros@central.ntua.gr.
[†] Institute of Physical Chemistry, NRCPS "Demokritos".
[‡] Department of Materials Science and Engineering, School of Chemical Engineering, National Technical University of Athens.
[§] Dutch Polymer Institute (DPI).
[⊥] Eduard-Zintl-Institut für Anorganische und Physikalische Chemie, Technische Universität Darmstadt, Petersenstrasse 20, D-64287 Darmstadt, Germany
[||] Dipartimento di Chimica, Università di Salerno.

10.1021/ma0700983 CCC: $37.00
Published on Web 04/19/2007

mistic ones. In this paper, this strategy is developed and tested for atactic polystyrene.

Coarse-graining has been central to hierarchical modeling of polymers since more than a decade. Strategies for coarse-graining have been reviewed.[3−5] In continuous coarse-grained models, several atoms are grouped together into "superatoms" connected by effective bonds.

Intramolecular and nonbonded potentials have to be defined among the superatoms in such a way that the coarse-grained model reproduces as closely as possible the structural and thermodynamic properties of the original atomistic model. Recently, several coarse-grained models have been proposed for PS. Milano and Müller-Plathe[6] proposed a model that preserves information on the stereochemical configuration. They studied the structural and dynamic properties of PS for chain molar masses up to 36000 g mol^{-1}. Sun and Faller[7] derived a coarse-grained model for PS based on the iterative Boltzmann inversion method.[8] They studied the dynamics of PS from the Rouse to the reptation behavior at various chain molar masses between 1500 and 25000 g mol^{-1} and determined the crossover to entangled dynamics. Unlike the model of ref 6, they did not account for different polymer stereosequences. Harmandaris et al.[9] recently proposed a coarse-graining and reverse-mapping scheme for PS. Their coarse-grained force field is based on atomistic simulations of isolated PS dimers and, considering as superatoms *R* and *S* pseudo asymmetric centers, is capable of differentiating between meso and racemic diads. Structure and chain dimensions of coarse-grained PS melts up to a molar mass of 10000 g mol^{-1} were presented.

In this work, the coarse-grained model for PS is the same as the one presented previously in ref 6. The bond angle potential and the nonbonded numerical potential have been further refined to achieve even better agreement with atomistic simulations. The ability of the model to account for different stereosequences is important, as this has an effect on the physical properties. High molecular weight chains up to 210000 g mol^{-1} are equilibrated at the coarse-grained level with the new potential via connectivity-altering MC moves. Sufficient equilibration of the system at this level is tested and verified. Thermodynamic and structural properties are calculated from the ensemble of coarse-grained configurations sampled, and compared against experimental data. By reducing the system of chains to topologically equivalent shortest paths via the CReTA algorithm,[10] a topological analysis of entanglements is performed. On the basis of the Kuhn length of reduced chains, an entanglement molar mass is predicted, which is in very good agreement with experimental estimates based on plateau modulus measurements. Subsequently, a reverse-mapping strategy is presented for generating relaxed united-atom configurations from the coarse-grained ones. Thermodynamic and structural properties are extracted from the reverse-mapped united-atom level and compared against experimental data.

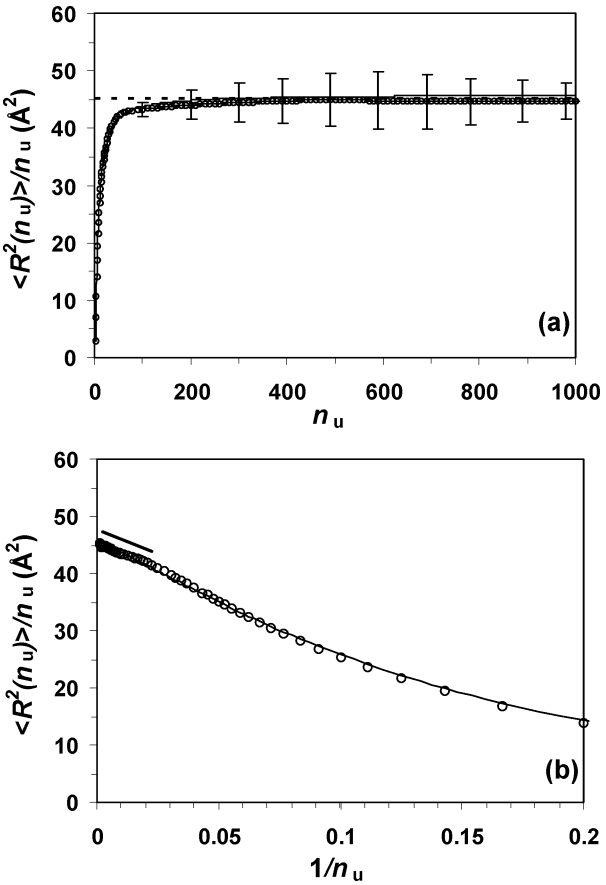

Figure 1. (a) Average squared end-to-end distance of subchains of length n_u diads ($\langle R^2(n_u)\rangle$) divided by n_u vs n_u for coarse-grained 1000-mer chains at 500 K. Some indicative error bars are shown. The dotted line is the SANS-based value for PS at 413 K. (b) $\langle R^2(n_u)\rangle/n_u$ vs $1/n_u$ for the same system. The short straight line indicates the linear behavior of $\langle R^2(n_u)\rangle/n_u$ (and hence C_n) as $1/n_u$ goes to zero. The analytical results for a freely rotating chain model (eq 1) consistent with the bond length and bond angle distributions of our CG chains are shown with thin lines in both plots.

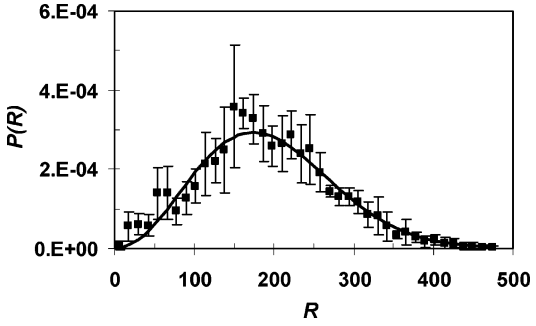

Figure 2. Normalized distribution of the end-to-end distance of coarse-grained 1000-mer chains in the melt at 500 K (symbols). This is approximated well by a Gaussian distribution (line).

2. The Coarse-Grained Model and Its Equilibration

Coarse-Grained Model. The scheme adopted here is very efficient for the representation of vinyl polymers, since one is able to keep information on stereochemical sequences along the polymer chain. Given a direction of the main chain, it is possible to assign an absolute configuration to each asymmetric carbon. The chain can be represented as a sequence of diads, each diad containing two asymmetric carbons. Depending on the absolute configuration of the asymmetric carbons, i.e., *RR* (or *SS*) and *RS* (or *SR*), the diads can be of the type *m* (*meso*) or *r* (*racemo*), respectively (please see Figures 1 and 2 of ref 6). The chain ends are always of the type *r* as far as the bonded potential is concerned, but their nonbonded potential is slightly different (after introduction of the ramp correction[4,8]); they are therefore denoted as a third type, *e*. A detailed description of the model can be found in ref 6. At the coarse-grained level, we simulate linear chains composed of three types of particles ("superatoms"), *m*, *r*, and *e*.

Force Field Refinement. The coarse-grained potential optimization aims at matching the distributions of three different bonds (*mm*, *mr*, *rr*), six bond angles (*mmm*, *mmr*, *mrm*, *mrr*, *rmr*, *rrr*), and the intermolecular pair distribution functions extracted from atomistic simulations. The approach, as reported in ref 6, involves the use of Gaussian based analytical potentials for bonds and angles and a tabulated numerical potential for the nonbonded interactions, obtained by the iterative Boltzmann inversion (IBI) method.[8] The bond length potential used here is the same as reported in ref 6. The bond angle potentials have been further refined in order to better reproduce the target distributions, extracted from all-atom simulations[11] of a 9mer fluid at 500 K and 1 bar. The parameters of the refined bond angle potentials are reported in the Supporting Information deposited with this article. Coarse-grained torsional potentials were neglected, as in ref 6. The coarse-grained nonbonded potential of ref 6, derived from the same atomistic force field[11] as in ref 6, was re-parametrized through more extensive IBI calculations in order to match better the system structure and pressure. The resulting numerical potentials are given in the Supporting Information. The interested reader should be able to reproduce all coarse-grained simulations reported in this work using the Supporting Information and the bond length potentials given in ref 6. The introduction of a refined coarse-grained force field in this work should not cast doubts on the earlier coarse-grained simulations presented in ref 6. All results discussed and conclusions reached in ref 6 remain valid under the refined potential.

In principle, there is a one-to-one correspondence between a pair potential and the pair correlation function obtained from it. It is, however, a common observation in IBI simulations that two visibly different pair potentials can produce indistinguishable pair correlation functions.[4,12] To address this point, Jain et al.[13] have performed IBI on simple model liquids (Lennard-Jones, WCA, and square-well). They showed in all cases that the generating pair potential was recovered, albeit at a very sluggish convergence rate. It took several thousand iteration cycles to recover the potential, while the pair correlation function was converged in but a few cycles. Convergence was about an order of magnitude faster, when thermodynamic targets were included by a scheme derived from our ramp correction.[4,8] This shows on one hand that obtaining the unique thermodynamically consistent potential presents a slow converging or possibly ill-conditioned numerical problem, even for the simplest model fluids. On the other hand, obtaining a potential which satisfies structure and thermodynamics and is useful for practical work, is not hard at all.

Coarse-Grained Simulations. The atactic polystyrene prepared by the usual technique of free radical polymerization is slightly syndiotactic; typically, the percentage of *m* diads from NMR analysis is between 40 and 50. The origin of this can be ascribed to the slightly higher stability of the syndiotactic chain. In this work, monodisperse melts of atactic PS chains with 46% meso diads and with chain lengths of 9, 100, 220, 350, 500, and 1000 coarse-grained sites (diads) were simulated in the *NPT* ensemble at $T = 500$ K and $P = 1$ bar. The chains in the initial configurations were built stepwise as follows. At each step a site type was chosen according to the overall probability of meso and racemo diads. A bond angle was chosen according to a probability resulting from the bond angle potential for the specific angle type and the segment was placed, accordingly, on a circle forming the base of a cone with apex at the previously placed site and side length equal to the average CG bond length of $l_{CG} = 2.46$ Å. The nonbonded energy of the segment with the already placed sites was checked, and if it did not exceed a certain value, the buildup continued. Otherwise, a new bond angle was chosen and the above procedure was repeated. If, after a certain number of iterations, all attempts to grow the chain failed, the head of the chain was placed elsewhere in the box and the above cycle was repeated. The choice of the Monte Carlo moves, which are discussed below, and the softness of the nonbonded potential permit a rapid relaxation of the initial configurations even at high chain lengths. The number of parent chains for each model system was 15, 14, 7, 4, 4, and 8, respectively. In addition, a big system containing 8 chains of 2000 sites each (molar mass 208316 g mol^{-1}) was simulated at $T = 413$ K. Although the potential was parametrized at 500 K, it is believed that its use in CG simulations at 413 K is legitimate. Temperature changes, at about the same density, do not affect the potential as much as concentration or density changes. This has been aptly demonstrated in a recent coarse-graining of polyethylene, by the same method as the one used here, where the effective coarse-grained potentials obtained from atomistic simulations 200 K apart differed by no more than 1 k_BT.[14] The sample at 413 K was used for topological analysis purposes, as will be discussed later. This system was also analyzed for its thermodynamic and conformational properties; results will be shown in the same figures as those from the other systems, only with a different symbol because of the different temperature. It is, however, expected, and it has been shown[15] that in the melt in the temperature range 393−513 K, the polymer does not exhibit a significant change in chain dimensions.

Equilibration Efficiency. The ability to equilibrate high molar mass chains at the coarse-grained level was one of the main objectives of this work. For this purpose, connectivity altering moves,[1,2] such as double bridging (DB), and intramolecular double rebridging (IDR), were employed in Monte Carlo simulations of linear chains of three types of sites, *m*, *r*, and *e*. In the DB move, two trimers are excised from two chains of equal length and two new trimer bridges are constructed, leading to two new chains of the same length but of drastically different conformations. In the IDR move, the two trimers belong to the same chain, and so the internal conformation of the chain is rearranged. Other types of moves were also employed: flips, rotations, concerted rotations, and volume fluctuations. The attempting rates of moves are of the same order as given in ref 2 for the long chain systems.

As a criterion of equilibration of the chain conformations one may use the quantity $\langle R^2(n_u)\rangle/n_u$, where n_u is the number of diads (repeat units) in a subchain and $R^2(n_u)$ is the squared end-to-end distance of the subchain. It has been shown[16] that, for well equilibrated chains, $\langle R^2(n_u)\rangle/n_u$ increases monotonically with n_u until it reaches a plateau. In Figure 1a, $\langle R^2(n_u)\rangle/n_u$ is shown as a function of n_u for a system containing 8 chains of 1000 diads each, at $T = 500$ K. For $n_u > 200$, an asymptotic value is reached of approximately 45 Å^2, which corresponds to $\langle R^2\rangle/M$ equal to 0.43 Å^2 g^{-1} mol, with M being the molar mass. This is in excellent agreement with the small-angle neutron scattering (SANS)-based value (shown with the dotted line) of $\langle R^2\rangle/M = 0.434$ Å^2 g^{-1} mol given for PS at $T = 413$ K.[17]

It is instructive to examine the chain length dependence exhibited by $\langle R^2(n_u)\rangle/n_u$ in Figure 1a. Along with simulation data in this figure we show the theoretical curve for a freely rotating chain[18] with $n_u - 1$ bonds, each of length $l_u = l_{CG} = 2.46$ Å, and bond angle θ_u satisfying $\cos\theta_u = \overline{\cos\theta_{CG}}$, with

$\overline{\cos\theta_{CG}} = -0.77$ being an average over all bond angle distributions of the CG model:

$$\frac{\langle R^2(n_u)\rangle}{n_u} = \left\{\frac{1-\cos\theta_u}{1+\cos\theta_u}\frac{n_u-1}{n_u} + \frac{2\cos\theta_u[1-(-\cos\theta_u)^{n_u-1}]}{(1+\cos\theta_u)^2}\frac{1}{n_u}\right\} l_u^2 \quad (1)$$

Comparing our CG model chains to a freely rotating chain model is reasonable, since they are devoid of torsional potentials. As seen in Figure 1a, the freely rotating chain model, eq 1, provides an excellent description of our CG melt simulation results.

For large chain lengths, eq 1 predicts that $\langle R^2(n_u)\rangle/n_u$ should become linear in $1/n_u$, with slope $l_u^2(2\cos\theta_u - 1 + \cos^2\theta_u)/(1+\cos\theta_u)^2$ and intercept at the origin $l_u^2(1-\cos\theta_u)/(1+\cos\theta_u)$. This is tested in Figure 1b. Clearly, the freely rotating chain model provides a good description of simulation data not only in the long-chain linear region, but throughout the range of subchain lengths examined in Figure 1b. The persistence length derived from mapping CG melt chains to freely rotating chains is $l_u/(1+\cos\theta_u) = 10.7$ Å; this is consistent with the characteristic ratio values discussed below.

The observed agreement between CG melt subchain dimensions and the freely rotating chain model, eq 1, provides strong indication that equilibration of conformations has been achieved at all length scales. Furthermore, predicted chain and subchain dimensions are in excellent agreement with experiment.

Figure 2 presents the normalized distribution of the chain end-to-end distance R for the 1000-mer system at 500 K. The simulation results are very well (within the error bars) approximated by the analytical expression for a chain whose end-to-end vector follows a Gaussian distribution,[18] shown as a solid line in Figure 2:

$$P(R) = 4\pi R^2 W(R) = 4\pi R^2\left(\frac{3}{2\pi\langle R^2\rangle}\right)^{3/2}\exp\left(-\frac{3R^2}{2\langle R^2\rangle}\right) \quad (2)$$

The average $\langle R^2\rangle$ derived from the fit of the Gaussian distribution to the simulation points is 45000 Å^2. From this one extracts a value of $\langle R^2\rangle/M$ equal to 0.43 Å^2 g^{-1} mol, in excellent agreement with the subchain analysis presented above and with SANS measurements.

Figure 2 provides further evidence that the chains in the melt are close to unperturbed and have correct dimensions. For long unperturbed chains one has a ratio of moments[18] $\langle R^4\rangle/\langle R^2\rangle^2 = 5/3$, which agrees well with the value 1.6 found from the simulation.

3. Coarse-Grained Simulation Results

Thermodynamic Properties and Conformation. The CG *NPT* simulations at $T = 500$ K and $P = 1$ bar converged to a density of 0.97 ± 0.02 g cm^{-3} for chain lengths longer than 100 units. Höcker et al.[19] proposed an equation of state that reproduces within $\pm(1\times10^{-4})$ g cm^{-3} the experimental densities of a nearly monodisperse sample of atactic PS of molar mass 51 000 g mol^{-1} for temperatures up to 230 °C. For $T = 500$ K, this equation of state gives $\rho = 0.95$ g cm^{-3}. An experimental value of 0.97 g cm^{-3} is reported in ref 17 for $T = 413$ K. (The same value is also produced by the aforementioned equation of state for this temperature.)

The isothermal compressibility κ_T was calculated from the volume fluctuations of the coarse-grained model in the *NPT* ensemble via the following relationship:

$$\kappa_T = \frac{1}{k_B T}\frac{\langle V^2\rangle - \langle V\rangle^2}{\langle V\rangle} \quad (3)$$

κ_T was found equal to 2.5×10^{-2} MPa^{-1} for chain lengths longer than 100 units. Experimental values for κ_T of PS are $(5.3-11.3)\times10^{-4}$ MPa^{-1} in the temperature range T_g to 593 K.[20] The large discrepancy (at least 1 order of magnitude) underlines the fact that coarse-grained potentials optimized through the IBI method at a specific pressure (here, 1 bar) cannot be ported reliably to different pressures; the CG interactions they lead to are too soft to reflect the true compressibility of the material. Alternative coarse-graining schemes that overcome this problem do exist,[21] but are considerably more laborious, as they invoke multidimensional pretabulation/interpolation schemes for interactions between nonspherical moieties.

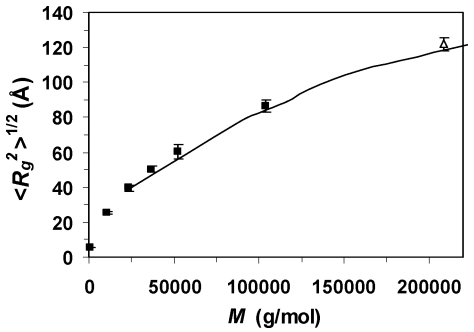

Figure 3. Average radius of gyration of the coarse-grained chains as a function of molar mass M in the melt at 500 K (filled symbols). With the open symbol is shown the result for the 2000-mer chains at a different temperature (413 K). The continuous line is neutron-scattering results for high molar mass a-PS in the bulk.[22]

The calculated root-mean-square radius of gyration $\langle R_g^2\rangle^{1/2}$ as a function of M is shown in Figure 3. Neutron scattering results[22] for monodisperse PS of M ranging from 21000 to 1100000 g mol^{-1} in the bulk at 393 K have also been drawn (thin line) for comparison over the M scale of interest. Very good agreement is observed for all the molar masses examined.

The mean squared end-to-end distance R^2 has been calculated for different chain lengths, and from this the characteristic ratio C_n has been extracted as a function of chain length n:

$$C_n = \langle R^2\rangle/(nl^2) \quad (4)$$

where l is the average skeletal bond length, taken equal to 1.53 Å, and n is the number of skeletal bonds per chain. (Note: actual chemical bonds, and not coarse-grained bonds, are counted in this definition.) The results are shown in Figure 4. C_n reaches a plateau of approximately 10 (±1) for all chain lengths larger than 220 repeat units that were examined here. Boothroyd et al.[15] reported C_∞ values measured by SANS on high molecular weight PS samples in the range $(8.7-9.6) \pm 4\%$ over the temperature range 393−513 K. This is in good agreement with the predictions of the model for the temperatures under consideration (413 and 500 K). The line almost connecting the simulation points in Figure 4 is the prediction of the freely rotating chain model (eq 1 above) with $n = 2n_u + 2$. Clearly, simulation results for the chain length dependence of the characteristic ratio from monodisperse melts of various molar masses are in excellent agreement with the freely rotating chain model, as well as with results from the analysis of subchains. This confirms that chains in our CG melts are well equilibrated and adopt close to unperturbed conformations.

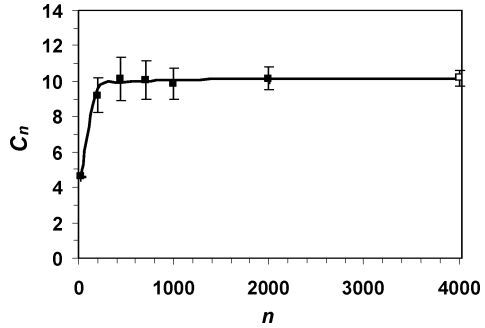

Figure 4. Characteristic ratio from coarse-grained simulations as a function of chain length n at 500 K. The open symbol refers to a different temperature ($T = 413$ K). The drawn line is the prediction of the freely rotating model.

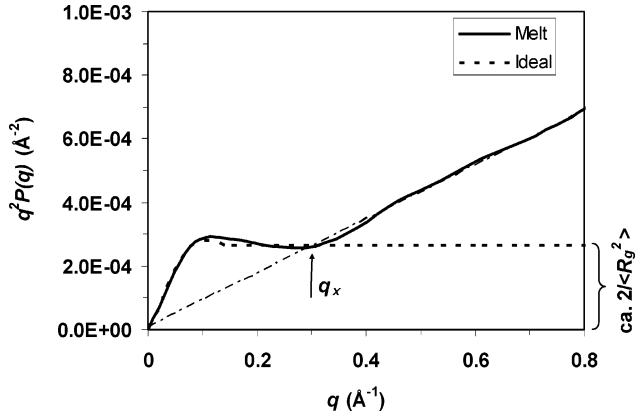

Figure 5. Kratky plot calculated from the single chain scattering intensity of coarse-grained 1000-mer chains in the melt at 500 K. The dotted line corresponds to an ideal Gaussian coil. The long-dashed line that passes through the origin intersects the ideal plateau at q_x, from which the persistence length can be estimated.

The single-chain scattering intensity[18] $I(q)$ of a 1000-mer chain in the melt at 500 K and 1 bar was calculated next from the Fourier transform of the total radial distribution function of all sites along the chain. The Debye scattering function $P(q)$ was obtained as $I(q)/I(0)$. $P(q)$ takes values between 0 and 1. Figure 5 shows $q^2P(q)$ vs q; it is the Kratky plot, used to extract chain dimensions and conformational characteristics from small-angle neutron scattering measurements with labeled chains. The Kratky plot of an ideal Gaussian coil with the same $\langle R_g^2 \rangle$ as our melt chains is shown in the same figure with a dashed line. This is calculated via the following relationship:[18]

$$P(q)_{\text{idealcoil}} = \frac{2}{\upsilon^2}[\upsilon - 1 + \exp(-\upsilon)],\ \upsilon = q^2\langle R_g^2 \rangle \quad (5)$$

The heights of the plateaus reached by the melt chains before the linear rise observed at large q and by the Gaussian coil are approximately equal to $2/\langle R_g^2 \rangle$. Using these heights, one extracts $\langle R_g^2 \rangle = 7490$ Å^2, which actually coincides with the value calculated by direct analysis of the melt chain configurations (see Figure 3). The straight line that passes from the origin and follows the linear rise of the melt curve at high q intersects the plateau at $q_x = 0.29$ Å. From this intersection point, it is possible to estimate the persistence length[18] as $l_p \equiv 2.3/q_x = 7.9$ Å. Hence, the Kuhn length of the melt chains is estimated as $l_K = 2\ l_p = 15.\ 8$ Å and the characteristic ratio as

$$C_\infty = \frac{l_K \sin\left(\frac{\theta}{2}\right)}{l} \quad (6)$$

If we take the bond length l equal to 1.53 Å for the backbone of an atomistic PS chain and the bond angle θ equal to 114° we obtain $C_\infty = 8.7$, which is in reasonable agreement with the value we found above by real-space analysis of the conformations, with previous calculations based on the same coarse-grained model,[6] and with experiment.

Entanglements. Topological analysis of coarse-grained PS has been performed by using the CReTA (contour reduction topological analysis) algorithm.[10] CReTA reduces a dense system of polymer chains[23] to the corresponding system of primitive paths (PPs). The latter are constructed as shortest paths,[23] which are under the same topological constraints as the original chains. The algorithm fixes chain ends in space, and by prohibiting chain crossing, it minimizes (shrinks) simultaneously the contour lengths of all chains, until they become sets of rectilinear strands coming together at the nodal points ("entanglements") of a network. As the algorithm proceeds, and in order to facilitate contour reduction through the removal of unentangled loops for the system, chain thickness is progressively reduced toward a zero value. The final thickness used for acquiring the results presented below was 0.118 Å. Extrapolation of the results to a zero thickness[10] would slightly increase our estimates for the entanglement molar mass M_e, and the tube diameter d.

On the basis of the tube model,[23] primitive paths are considered as Gaussian coils and an entanglement strand is identified with the Kuhn segment of the primitive path. M_e and d correspond to the molar mass and the end-to-end distance of a Kuhn segment of the PP. In our case, the relevant quantities are the number of diads (repeat units) in a PP Kuhn segment, N_e, and the PP Kuhn length d, which are determined from the relations

$$d = \frac{\langle R^2 \rangle}{\langle L_{pp} \rangle},\ N_e = N\frac{\langle R^2 \rangle}{\langle L_{pp} \rangle^2} \quad (7)$$

where $\langle L_{pp} \rangle$, $\langle R^2 \rangle$ are the PP contour length and squared end-to-end distance, respectively, calculated here as ensemble averages over all chains present. N is the number of chain backbone repeat units, or diads for our coarse-grained PS model.

We have analyzed monodisperse coarse-grained configurations of PS, with 8 chains of 2000 diads each, equilibrated at 413 K. N_e was estimated to be 124 diads, and since the average molar mass of a diad is 104.15 g mol,$^{-1}$ the corresponding entanglement molar mass M_e is 12915 ± 300 g mol^{-1}. This value is in good agreement with experimental estimates based on plateau modulus measurements. A value of 13309 g/mol (128 diads) at $T = 413$ K is reported by Fetters et al.,[17] and of 14800 g/mol (142 diads) by Liu et al.[24] The latter value was calculated from an average plateau modulus taken by measurements on various molecular weight samples, at slightly higher temperatures (by 30−50 K).

Another quantity which has been found to correlate with M_e of a large number of flexible polymers is the packing length,[17] $p = 1/(\nu\langle R^2 \rangle)$, where ν is the number density of chains. The packing length is controlled by monomer packing (density) and chain dimensions (stiffness) in the melt state. Our p estimate is 3.94 Å, in very good agreement with the experimental value of 3.95 Å reported in ref 17. The reptation tube diameter d, calculated through eq 9, is 75.8 ± 1.5 Å, in very good agreement with the value of 76.5 Å reported in ref 17, calculated through the packing length model.

In the topological analysis performed in ref 10 it was found that the length scale defined by the average mesh size of the

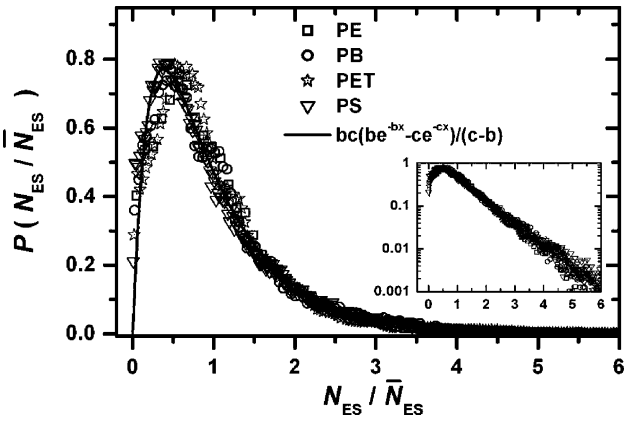

Figure 6. Normalized distribution of reduced entanglement network mesh size (step length of PPs) $N_{ES}/\bar{N}_{ES}$ for PE, PB, PET, and PS, where N_{ES} is measured in number of chain backbone chemical units, diads in the case of PS. The inset shows the same data in semilog coordinates, where superposition is better displayed.

reduced entanglement networks, i.e., the average step size of the PPs (shortest paths), is smaller than the length scale where the PPs become random walks, i.e., the "Kuhn scale" of the PPs, which is related with the entanglement molar mass (eq 7). This happens because exponentially decaying orientational correlations exist[10] between neighboring steps of PPs. Figure 6 shows the reduced normalized distribution $P(N_{ES}/\bar{N}_{ES})$ of the mesh size N_{ES} divided by its average value, for the corresponding entanglement networks of PS and other polymer melts, such as Polyethylene (PE), *cis*-1,4 polybutadiene (PB) and Poly(ethylene terephthalate) (PET). For PS, $\bar{N}_{ES} = 48$ diads. Data for PE, PB are from simulations of ref 10 and data for PET are from simulations of Kamio et al.[25] It is seen that the data are superposable. This is a direct consequence/demonstration[10] of the fact that the underlying topology of these flexible polymers, as determined by reducing polymer specimens to networks of interpenetrating shortest paths, is statistically similar. The solid line in Figure 6 is a fit to all data with a functional expression involving the difference of two exponentials. This normalized distribution can be interpreted[10] as resulting from a stochastic point process which generates topological constraints along the sequence of monomer units of a polymer chain. Other reduced distributions (not shown here) describing the underlying topology of PS are the same as those presented in ref 10.

5. Reverse Mapping

United-Atom Force Field. The equilibrated coarse-grained configurations were mapped to detailed configurations using a united-atom model representation without partial charges, shown in Table 1. This potential is different from the atomistic potential used to generate the target distributions[6] for the optimization of the coarse-grained model. Our choice to reverse map into a united-atom model was motivated by our use of this model in other computations (concerning relaxation in the glassy state). Our experience has been that the united-atom model does a reasonable job predicting structure, volumetric properties, elastic constants and stress−strain behavior in the glassy state. This creates the interesting possibility of reverse mapping the coarse-grained representation into a different detailed representation from the one that was used to derive it. If both the coarse-grained model and the atomistic model into which reverse mapping is performed are good models for polystyrene melts under the considered temperature and pressure conditions, the reverse mapping should be successful.

PS chains were assumed to have a symmetric chemical formula from both ends, of the type $CH_3-CH-(C_6H_5)-[CH_2-CH-(C_6H_5)-]_{n_u}-CH_3$, where n_u is the number of diads. For simplicity, the CH_3 ends were taken as CH_2. The united-atom potential was from Mondello et al.[26] with some modifications as shown in Table 1. The cutoff distance was extended to 9 Å. Unlike the potential in ref 26, the bond lengths were not fixed but allowed to fluctuate around their equilibrium values via a harmonic potential with spring constants taken from ref 27, but not attenuated by 4 as was done in ref 27 in order to increase the MD integration time step. Also, instead of maintaining the planarity of the rings with a phenyl ring out-of-plane bending potential, the valence angles in the rings were allowed to fluctuate via a harmonic potential as was implemented in ref 28. Similarly to ref 28, a 2-fold torsional potential was implemented for the rotations around the aromatic bonds. Finally, an improper angle potential was used in order to prevent reversals of chirality of the skeletal carbons, as proposed in ref 29. This potential proved to be more effective than that of ref 26 in maintaining the stereochemical configuration of the aliphatic CH during the optimization of the structure, because it goes to infinity when the four carbons around CH(aliph) tend to collapse onto a plane, driving the geometric quantity f_{chir} (see Table 1) to 1. The potential of Table 1 assigns the *trans* conformation to 0°.

Structure Optimization. Milano and collaborators[30] proposed a reverse mapping strategy for PS that is basically geometrical and uses quaternions to dock atomistic diads on the coarse-grained configurations. In the present work, the structure optimization is achieved through energy minimization. More specifically, an initial guess united-atom configuration was created purely geometrically, by placing all achiral backbone carbons on their respective coarse-grained positions and connecting them via chiral carbons. The bond lengths and bond angles of the chiral carbons were placed according to the equilibrium values of Table 1, allowing small deviations. The first chiral carbon of each chain was assigned randomly an absolute configuration, since this is not determined by the coarse-grained model, and the rest of the chiral carbons were placed according to the chirality of the diads. The phenyl rings were constructed planar and normal to the backbone. Initially, the nonbonded interactions were turned off and the configuration was optimized via Monte Carlo flip moves.[31] A flip move displaces an inner skeletal segment of the chain along the locus (circle) defined by the lengths of the two bonds adjacent to the segment. The moves employed flipped (a) an achiral carbon atom (CH_2 group, initially placed at a coarse-grained diad interaction site) and (b) a chiral carbon (one carrying a phenyl) to a new position on the circumference of a circle drawn perpendicular to the line connecting the carbons flanking it on either side. Initially the structure was optimized with respect to the bonded potential (bond lengths, bond angles, torsions, and improper angles).

This stage of the calculations optimizes the bonded interaction energy. During the whole MC optimization, moves leading to a $\bar{g}$ (gauche-bar)[18] conformation were forbidden. This tends to eliminate any $\bar{g}$ conformations that may be present in the initial guess reverse-mapped configuration. The chirality of the asymmetric carbons was maintained with a simple harmonic potential instead of the form listed under item 7 in Table 1, the latter being more suitable for continuous changes of the structure during MD:

$$V_\varphi = k_\varphi(\varphi - \varphi_0)^2 \tag{8}$$

Table 1. United-Atom Force Field for PS Used in Reverse Mapping (Chain Structure: $CH_3-CH-(C_6H_5)-[CH_2-CH-(C_6H_5)-]_{n_u}-CH_3$)

1. Nonbonded Interactions

$V_{nb} = \epsilon[(r_0/r)^{12} - 2(r_0/r)^6]$; $\epsilon = (\epsilon_1\epsilon_2)^{0.5}$	$r_0 = (r_{0,1} + r_{0,2})/2$
$\epsilon = 0.12$ kcal mol^{-1}	$r_0 = 4.321$ Å for CH_2
$\epsilon = 0.09$ kcal mol^{-1}	$r_0 = 4.153$ Å for aliphatic CH
$\epsilon = 0.12$ kcal mol^{-1}	$r_0 = 4.153$ Å for aromatic C and CH
cutoff distance = 9 Å	

2. Bond Lengths

$V_l = k_l(l - l_0)^2$	
$k_l = 317$ kcal mol^{-1} Å^{-2}	$l_0 = 1.53$ Å for aliphatic CH_2-CH
$k_l = 317$ kcal mol^{-1} Å^{-2}	$l_0 = 1.51$ Å for CH(aliph)-C(arom)
$k_l = 525$ kcal mol^{-1} Å^{-2}	$l_0 = 1.40$ Å for CH(arom)−CH(arom)

3. Bond Angles

$V_\theta = k_\theta(\theta - \theta_0)^2$	
$k_\theta = 60$ kcal mol^{-1} rad^{-2}	$\theta_0 = 109.5°$ for aliphatic $CH_2-CH-CH_2$
$k_\theta = 63$ kcal mol^{-1} rad^{-2}	$\theta_0 = 109.5°$ for aliphatic $CH-CH_2-CH$
$k_\theta = 60$ kcal mol^{-1} rad^{-2}	$\theta_0 = 109.5°$ for CH_2(aliph)−CH(aliph)-C(arom)
$k_\theta = 70$ kcal mol^{-1} rad^{-2}	$\theta_0 = 120°$ for CH(aliph)-C(arom)−CH(arom)
$k_\theta = 72$ kcal mol^{-1} rad^{-2}	$\theta_0 = 120°$ for CH(arom)−CH(arom)−CH(arom)

4. Backbone Torsion (X−CH(aliph)−CH_2(aliph)−X)

$V_\varphi = k_\varphi(1 - \cos 3\varphi)$

$k_\varphi = 1.4$ kcal mol^{-1}

(trans taken as $\varphi = 0$)

5. Torsion CH_2(aliph)−CH_2(aliph)−CH(arom)−CH(arom)
(Phenyl Ring Torsion Around CH(aliph)−C(arom))

$V_\varphi = k_\varphi(1 + \cos 2\varphi)$

$k_\varphi = 1$ kcal mol^{-1}

(trans taken as $\varphi = 0$)

6. Torsion CH(arom)−CH(arom)−CH(arom)−CH(arom)

$V_\varphi = k_\varphi(1 + \cos 2\varphi)$

$k_\varphi = 12.9$ kcal mol^{-1}

(trans taken as $\varphi = 0$)

7. Improper torsion (C(arom)−CH(aliph)−CH_2(aliph)−CH_2(aliph))
(To Maintain Chirality)

$V^{chir}(f_{chir}) = [\kappa/(1 - f_{chir})] - [\kappa f_{chir}^2/(1 - \delta)^3] + [\kappa(3\delta - 1)f_{chir}/(1 - \delta)^2] - [\kappa(3\delta^2 - 3\delta + 1)/(1 - \delta)^3]$

$f_{chir} = (\cos^2\alpha + \cos^2\beta + 2\cos\alpha\cos\beta\cos\theta)/\sin^2\theta \leq 1$

$\kappa = 0.05$ kcal mol^{-1} $\delta = 0.4$

bond angles

$\pi-\alpha$: CH_2(aliph)−CH(aliph)−C(arom)

$\pi-\beta$: C(arom)−CH(aliph)−CH_2(aliph)

$\pi-\theta$: CH_2(aliph)−CH(aliph)−CH_2(aliph)

where φ is the improper dihedral angle whose sign determines the chirality (C(arom)−CH(aliph)−CH_2(aliph)−CH_2(aliph)) and k_φ was taken arbitrarily equal to 1 kcal mol.$^{-1}$ φ_0 has an absolute value of 60° (the trans conformation corresponds to 0°) and the same sign as φ. The φ_0 value ensures a tetrahedral structure for the chiral carbons. The nonbonded interactions were turned on progressively by augmenting the Lennard-Jones parameters r_0 of Table 1 during the flip MC relaxation process up to 90% of their final values. As r_0 increase, flip moves induce only local "vibrational" motions around the current positions and the relaxation of the structure becomes progressively slower. In order to reach a final reverse-mapped configuration, collective relaxation by MD was undertaken; the configuration was loaded on the MD program large-scale atomistic/molecular massively parallel simulator (LAMMPS)[32] with the force field of Table 1. Thus, 2−5 ps of an *NVT* run at the same density and temperature as the corresponding coarse-grained system were sufficient for relaxing the system at the prescribed conditions. Stabilization of the average energy and its components (stretching, bending, torsional, nonbonded) within 1% of their final values was used here as a criterion for relaxation. Figure 7 shows an unfolded 350-mer chain in its coarse-grained representation, and the same chain in atomistic detail after the reverse mapping. The whole optimization procedure displaces the coarse-grained diad centers (equivalently, the corresponding CH_2 sites) by 0.5−0.8 Å on the average per site. The atomistic system is not moved away from the underlying coarse-grained system because of the strong steric hindrances it experiences; this gives one an idea of how difficult it is to equilibrate atomistic PS melt configurations from scratch, or to escape from distorted local conformations.

The MC flip relaxation procedure was chosen because of the convenience it offers to conserve the system chirality, which is difficult to conserve with MD alone when the system has excessive overlaps and is far from equilibrium. Also, it makes it possible to optimize the torsion angle distribution of the reverse-mapped system by prohibiting the improbable $\bar{g}$ conformations. Less elaborate reverse mapping schemes produce skeletal torsion angle distributions which tend to be symmetric between g (gauche) and $\bar{g}$, as discussed below.

Thermodynamic Properties and Structure of the Reverse-Mapped Configurations. *NVT* MD runs conducted on the reverse-mapped configurations at the same density and temperature as the corresponding coarse-grained systems fluctuated around $P = 1$ bar. This means that the atomistic structures were able to converge to the same pressure as the coarse-grained systems.

The solubility parameter δ was calculated for three reverse-mapped structures with 350 diads per chain. For this calculation the intermolecular interactions for each system were summed, averaged, and divided by the average box volume to obtain an estimate of the cohesive energy density. The square root of the

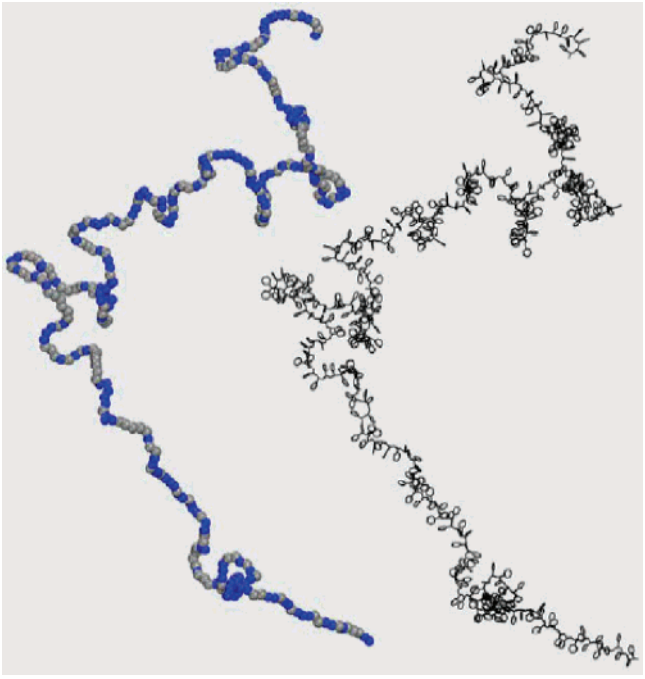

Figure 7. Illustration of the reverse-mapping scheme. On the left is an unfolded 350-mer chain with *m* (blue) and *r* (gray) segments. On the right is the reverse-mapped atomistic chain.

cohesive energy density averaged over all three structures, δ, was found to be equal to 14.5 ± 0.5 $(J/cm^3)^{1/3}$ at $T = 500$ K. Experimental values for PS range from 17.4 to 19 $(J/cm^3)^{1/2}$ at $T = 298$ K.[20] This discrepancy of about 20% is rather large and is partly due to the temperature difference (the cohesion of the polymer drops as the temperature rises and so δ should decrease as well). A short-chain structure (made from a single 80-mer single parent chain) equilibrated directly with MD at 500 K gave an even lower solubility parameter. This structure resulted from a model configuration at ambient conditions submitted to annealing cycles realized by increasing the temperature by 50 K each time and simulating for 4 ns under constant pressure, until the desired temperature was reached. The initial 80-mer structure was provided by Prof. Alexey Lyulin, along with an MD program which implements the force field of ref 28. Unlike ref 28, where all bond lengths were kept fixed, the bond stretching potential of Table 1 was implemented during the annealing cycles. Again, stabilization of the average energy and all its components and also of the density within 1% of their final values was used as a criterion of equilibration for the 80-mer MD simulations.

The ability of the proposed strategy to generate realistic configurations of atactic PS was tested by comparing wide-angle X-ray diffraction patterns of PS[33] with the calculated scattering intensity, obtained via Fourier transform of the total radial distribution functions of the united-atom reverse-mapped structures. The atomic scattering factors[34] of two types of sites were used, i.e., (a) the $-CH_2-$ for the achiral carbons and the chain ends and (b) the $=CH-$ for the chiral carbons and the phenyl ring carbons. As shown in Figure 8, atactic PS exhibits a first peak, known as the "polymerization peak", at $q = 0.75$ Å^{-1}, which is absent from small-molar mass liquids such as styrene and benzene; a high peak at $q = 1.4$ Å^{-1} associated with segment correlations between neighboring chains; and a much lower peak at $q = 3.1$ Å^{-1}. The intensity of the first peak increases significantly with temperature. The calculated intensity for a reverse-mapped configuration of a 4-chain system of 350-mers at 500 K is shown in the same figure. The first peak

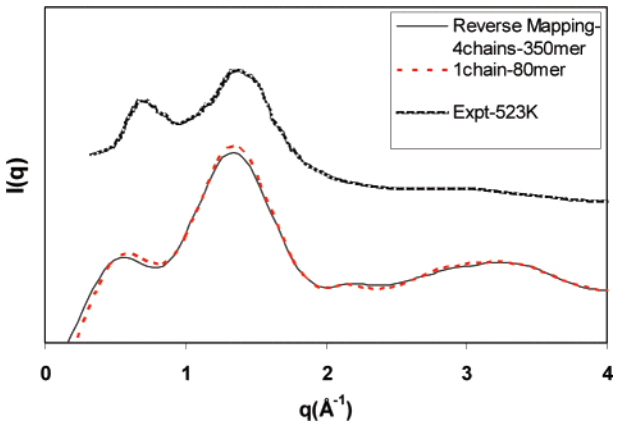

Figure 8. Calculated scattering intensity from a melt of reverse-mapped chains of 350mers at 500 K (continuous line) and from a small model melt system constructed from a single 80-mer parent chain at the same *T* (dotted line). Over the simulation results, with the thick dotted line, is shown the experimental X-ray scattering pattern of atactic PS at 523 K.[33]

appears at a lower *q*, around 0.6 Å^{-1}. The *interchain* peak appears at the same wavenumber as in experiment, and the third peak at approximately $q = 3.2$ Å^{-1}. In the same figure is shown the calculated intensity for a well- equilibrated small system, consisting of a single atactic PS "parent" chain with 80 monomers at the same temperature. The comparison with the reverse-mapped structure is excellent; this indicates that the discrepancies observed with respect to the experimental data, mainly the *q* at which the polymerization peak appears and the relative height of the two first peaks, are due to the force field and not to insufficient equilibration.

NMR measurements on atactic PS have helped gain insight into the conformations adopted by its chains. Suter and collaborators have shown[35,36] that considerable deviations may occur between experimental findings and predictions obtained from bulk atomistic model structures of PS; furthermore, they have proposed an algorithm for the generation of atomistic structures by an appropriate choice of the target conformational probabilities in the spirit of the RIS model. Having this in mind, the ability of the current scheme to generate atomistic configurations with correct conformational statistics was examined next. It was found that the mere inclusion of a torsional potential during the reverse mapping procedure did not suffice for the generation of reasonable torsional distributions. A high population of $\bar{g}$ angles resulted and a nearly symmetric distribution was obtained between g and $\bar{g}$. This can be understood as a result of the steric hindrances that can *lock* the system into energetically unfavorable conformations. For this reason, $\bar{g}$ conformations were excluded during the structure relaxation with flip MC; only in the final MD relaxation cycle were they allowed to occur. The resulting torsional distributions for a 4-chain system of 350-mers at 500 K are shown in Figure 9 for the *meso* and the *racemo* diads. Each distribution is an average over 3 reverse-mapped configurations. In the same figure, with the dashed line, are shown the distributions obtained for a small system of an 80-mer subjected to a 4 ns *NPT* MD simulation at the same temperature. Details for the generation of the small system configuration have been given above.

The fusion of the trans and gauche states is apparently produced by the atomistic potential at this high temperature, since it is also present in the small system, whose torsion angle distribution is well equilibrated. Comparing the two curves for the *meso* and the *racemo* diads, we observe a higher population of $\bar{g}$ conformations in the reverse-mapped structures and a lower

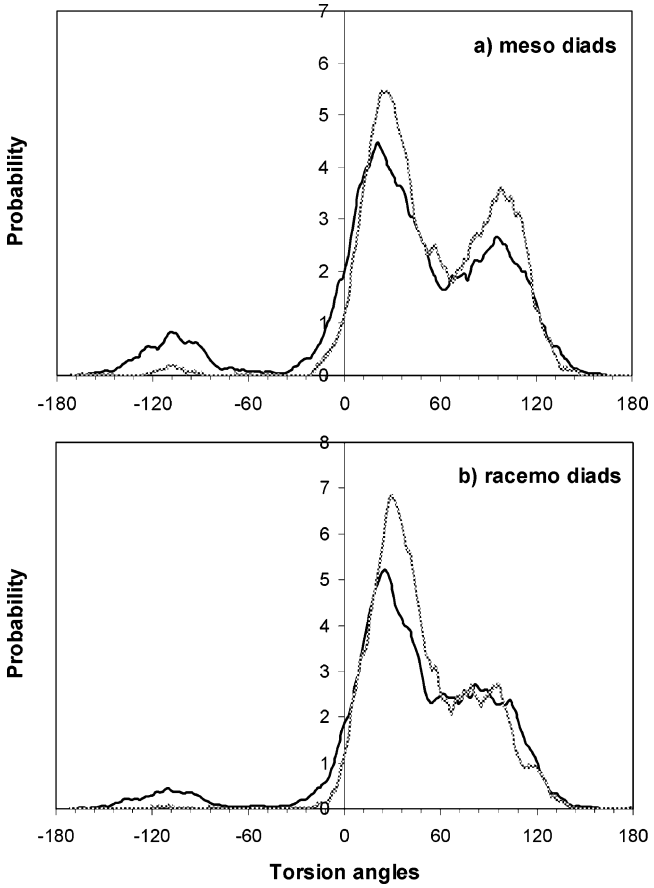

Figure 9. Average distribution of torsion angles for the meso and racemo diads over 3 reverse-mapped configurations of 350-mer chains in the bulk (continuous line) and of an atomistic 80-mer single parent chain system simulated by MD at the same *T* (dotted line).

percentage of trans states in the *racemo* diads. The overall content of trans conformations in the reverse-mapped structures is around 60%, which is in reasonable agreement with the experimental 68 ± 10% measured by NMR.[37] In the *racemo* diads of the reverse-mapped structures, successive angles in the *tt* (*trans*−*trans*) conformation are about 45%, while in the *meso* diads the *tg* (trans−gauche) or *gt* conformations are about 60%. The corresponding values of several RIS models[38] for a-PS that reproduce satisfactorily the distance factors found by NMR are 50% or more for the *tt* conformations of the *racemo* diads and 85% or more for the *tg* or *gt* conformations of the *meso* diads. The total percentage of $\bar{g}$ conformations in the reverse-mapped structures was 5−7%, while, according to RIS models, it should be less than 2%. Clearly, capturing the correct torsion angle distribution is a stringent test for reverse mapping from the coarse-grained representation adopted in this work, and further refinements in the coarse-grained model and/or reverse mapping algorithm would be desirable.

6. Conclusions

In this paper, we have outlined a strategy for simulating monodisperse long-chain atactic polystyrene melts at three levels: a coarse-grained one, wherein each diad along the chains is represented as a single interaction site, or "superatom"; a detailed one, employing a united-atom model representation for the polymer; and a mesoscopic level, wherein coarse-grained configurations are further reduced to entanglement networks by topological analysis. Results from all three levels have been presented. For the first time, melts of molar mass up to 210000 g mol^{-1} have been addressed in the simulations.

The coarse-grained simulations were based on the model of Milano and Müller-Plathe,[6] parametrized through an iterative Boltzmann inversion technique. The coarse-grained model was equilibrated at 500 or 413 K and 1 bar using connectivity-altering Monte Carlo moves[1,2] (double bridging, intramolecular double rebridging), along with flips, rotations, concerted rotations, and volume fluctuations. Chain conformations obtained through these coarse-grained simulations were found to be equilibrated at all length scales (Figure 1). Chain dimensions, as predicted from the mean square end-to-end distance and its distribution (Figure 2), from the mean square radius of gyration (Figure 3), from the characteristic ratio (Figure 4), and from the Kratky plot (Figure 5) were found to be in excellent agreement with available experimental evidence. This confirms that IBI-based coarse-graining in combination with connectivity-altering Monte Carlo is an extremely powerful strategy for equilibrating long-chain melts of moderately complex chemical constitution, an observation already made in the case of poly(ethylene terephthalate).[25] Melt densities from the coarse-grained MC simulations were in very good agreement with experimental densities at 1 bar. Melt compressibilities from the coarse-grained simulations were too high, however, indicating that IBI-based models should be used with caution at pressures far removed from those at which they were parametrized.

Well-equilibrated melt configurations sampled by coarse-grained MC were reduced to entanglement networks using the CReTA algorithm.[10] To our knowledge, this is the first time topological analysis is employed to predict the entanglement properties of polystyrene and of a realistic polymer with a large packing length; the ability to equilibrate long-chain melts in the coarse-grained representation via connectivity-altering MC is critical to the success of this effort. The Kuhn lengths of reduced chains (primitive paths) obtained through the CReTA procedure yielded an estimate of M_e equal to 12915 g mol^{-1} and of the entanglement tube diameter *d* equal to 75.8 Å. These estimates are in excellent agreement with experimental values derived from the plateau modulus.[17,24] The packing length *p* is also in almost perfect agreement with experiment, since the experimental density and chain dimensions are captured very well by the simulations. Thus, simulation results conform to the experimentally based correlation[17] $M_e \sim \rho p^3$. On the other hand, the mean molar mass of strands between successive entanglements (mesh size of the entanglement network, as determined by CReTA) is only ca. 40% of M_e. All these observations are in line with earlier topological analyses of united-atom polyethylene and *cis*-1,4 polybutadiene[10] and of coarse-grained poly(ethylene terephthalate),[25] making a-PS the fourth polymer where the CReTA analysis has been applied, successfully. The distribution of reduced entanglement strand lengths (Figure 6) falls on the same master curve with previously studied polymers; the curve can be envisioned as resulting from the convolution of two Poisson processes, as discussed in ref 10.

A new method has been proposed for reverse-mapping the equilibrated coarse-grained melt configurations to a detailed united-atom model of PS (Table 1). Detailed united-atom configurations were "threaded" through the coarse-grained chains and then relaxed at constant volume through local MC "flip" moves. Initially, only the bonded energy (contributions from bond lengths, bond angles, torsion and improper angles) were taken into account in the flip MC relaxation process. Subsequently, nonbonded interactions were gradually turned on. During the whole MC energy optimization process, $\bar{g}$ states were disallowed. This was found necessary in order to guide the

reverse-mapping process into a conformationally reasonable subspace of the configuration space of the detailed model. Reverse mapping was completed by 2−5 ps *NVT* MD runs. The entire reverse-mapping procedure displaced CH_2 sites from their original coarse-grained positions by 0.5 − 0.8 Å. The pressure of reverse-mapped configurations was around 1 bar, indicating that their volumetric properties are reasonable. Atomic packing in the reverse-mapped configurations, as quantified by the predicted X-ray diffraction pattern, is indistinguishable from that of 80-mer configurations equilibrated directly via MD using the same united-atom model, and in favorable agreement with experiment (Figure 8). The distributions of torsion angles in the reverse-mapped configurations depart considerably from those of an 80-mer melt equilibrated directly using the same united-atom model (Figure 9). Reverse-mapped torsion angle distributions exhibit a higher population of $\bar{g}$ states and less pronounced localization in the *tt* and *tg* pairs of states for *racemo* and *meso* diads, respectively. Predictions from the directly equilibrated 80-mer system are in better agreement with torsion angle populations extracted from NMR measurements.[35,36] This underlines the utility of torsion angle distributions as a stringent test for reverse-mapped structures and indicates that there is room for improvement in the coarse-grained model and/or reverse mapping algorithm.

Acknowledgment. This work was supported by the European Commission through an NMP STREP project, Contract NMP3-CT-2005-013644 (MULTIMATDESIGN). Additional support provided by the Dutch Polymer Institute, Project #430, is gratefully acknowledged. Prof. Alexey Lyulin, Dr. George Boulougouris, and Mr. Dimitris Tsalikis are thanked for the atomistic calculations on the single parent chain 80-unit atactic polystyrene structure, used in validating the reverse mapping procedure.

Supporting Information Available: A .txt file containing the numerical nonbonded potentials and text describing how the coarse-grained bonded and nonbonded potentials are obtained and a table of the bending potentials. This material is available free of charge via the Internet at http://pubs.acs.org.

References and Notes

(1) Karayiannis, N. Ch.; Mavrantzas, V. G.; Theodorou, D. N. *Phys. Rev. Lett.* **2002**, *88*, 105503.
(2) Karayiannis, N. Ch.; Giannousaki, A. E.; Mavrantzas, V. G.; Theodorou, D. N. *J. Chem. Phys.* **2002**, *117*, 5465.
(3) Baschnagel, J.; Binder, K.; Doruker, P.; Gusev, A. A.; Hahn, O.; Kremer, K.; Mattice, W. L.; Müller-Plathe, F.; Murat, M.; Paul, W.; Santos, S.; Suter, U. W.; Tries, V. *Adv. Polym. Sci.* **2000**, *152*, 41.
(4) Müller-Plathe, F. *Chem. Phys. Chem.* **2002**, *3*, 754; *Soft Mater.* **2003**, *1*, 1.
(5) Faller, R. *Polymer* **2004**, *45*, 3869.
(6) Milano, G.; Müller-Plathe, F. *J. Phys. Chem. B* **2005**, *109*, 18609.
(7) Sun, Q.; Faller, R. *Macromolecules* **2006**, *39*, 812.
(8) Reith, D.; Pütz, M.; Müller-Plathe, F. *J. Comp. Chem.* **2003**, *24*, 1624.
(9) Harmandaris, V. A.; Adhikari, N. P.; van der Vegt, N. F. A.; Kremer, K. *Macromolecules* **2006**, *39*, 6708.
(10) Tzoumanekas, C.; Theodorou, D. N. *Macromolecules* **2006**, *39*, 4592.
(11) Müller-Plathe, F. *Macromolecules* **1996**, *29*, 4782.
(12) Reith, D. Ph. D. Thesis, University of Mainz 2001.
(13) Jain, S.; Kumar, S. K. *Ind. Eng. Chem. Res.* **2006**, *45*, 5614.
(14) Vettorel, T.; Meyer, H *J. Chem. Theory Comput.* **2006**, *2* (3), 616.
(15) Boothroyd, A. T.; Rennie, A. R.; Wignall, G. D. *J. Chem. Phys.* **1993**, *99* (11), 9135.
(16) Auhl, R.; Everaers, R.; Grest, G. S.; Kremer, K.; Plimpton, S. J. *J. Chem. Phys.* **2003**, *119*, 12718.
(17) Fetters, L. J.; Lohse, D. J.; Richter, D.; Witten, T. A.; Zirkel, A. *Macromolecules* **1994**, *27*, 4639.
(18) Mattice, W. L.; Suter, U. W. *Conformational Theory of Large Molecules*; Wiley: New York, 1994.
(19) Höcker, H.; Blake, G. J.; Flory, P. J. *Trans. Faraday. Soc.* **1971**, *67*, 2251.
(20) Mark, J. E., Ed. *Polymer Data Handbook*; Oxford University Press: New York, 1999.
(21) Zacharopoulos, N.; Vergadou, N.; Theodorou, D. N. *J. Chem. Phys.* **2005**, *122*, 1.
(22) Cotton, J. P.; Decker, D.; Benoit, H.; Farnoux, B.; Higgins, J.; Jannink, G.; Ober, R.; Picot, C.; des Cloizeaux, J. *Macromolecules* **1974**, *7*, 863.
(23) Doi, M.; Edwards, S. F. *The Theory of Polymer Dynamics*; Clarendon: Oxford, U.K., 1986.
(24) Liu, C.; He, J.; van Ruymbeke, E.; Keunings, R.; Bailly, C. *Polymer* **2006**, *47*, 4461.
(25) Kamio, K.; Moorthi, K.; Theodorou, D. N. *Macromolecules* **2007**, *40*, 710.
(26) Mondello, M.; Yang, H.-J.; Furuya, H.; Roe, R.-J. *Macromolecules* **1994**, *27*, 3566.
(27) Han, J.; Boyd, R. H. *Polymer* **1996**, *37*, 1797.
(28) Lyulin, A. V.; Michels, M. A. J. *Macromolecules* **2002**, *35*, 1463.
(29) Greenfield, M. Ph.D. Thesis, University of California at Berkeley 1996.
(30) Santangelo, G.; Di Matteo, A.; Müller-Plathe, F.; Milano, G. *J. Phys. Chem. B* **2007**, *111*, 2765.
(31) Mavrantzas, G. V.; Theodorou, D. N. *Macromolecules* **1998**, *31*, 6310.
(32) Plimpton, S. *J. Comput. Phys.* **1995**, *1*, 117.
(33) Mitchell, G. R.; Windle, A. H. *Polymer* **1984**, *25*, 906.
(34) Narten, A. H. *J. Chem. Phys.* **1979**, *70*, 299.
(35) Robyr, P.; Gan, Z.; Suter, U. W. *Macromolecules* **1998**, *31*, 8918.
(36) Robyr, P.; Müller, M.; Suter, U. W. *Macromolecules* **1999**, *32*, 8681.
(37) Dunbar, M. G.; Novak, B. M.; Schmidt-Rohr, K. *Solid State NMR* **1998**, *12*, 119.
(38) Rehahn, M.; Mattice, W. L.; Suter, U. W. *Rotational Isomeric State Models in Macromolecular Systems*; Advances in Polymer Science 131/132; Springer: Berlin 1997.

MA0700983